Assessing the Impact of Time Correlation Uncertainty on Cycle Ambiguity Resolution for High Integrity Aviation Applications

Steven Langel, Samer Khanafseh and Boris Pervan
Illinois Institute of Technology

BIOGRAPHY

Steven Langel is a PhD candidate at the Illinois Institute of Technology whose research focuses on the design of high accuracy, high integrity navigation algorithms for aerospace applications. Specific research interests include carrier phase differential GPS navigation with cycle resolution, Kalman filtering with stochastic modeling uncertainty and the design of GPS / INS integration algorithms. Steven received his B.S. degree in mechanical and aerospace engineering from the Illinois Institute of Technology in 2006.

Samer Khanafseh is a research assistant professor at the Illinois Institute of Technology whose work involves high accuracy and high integrity navigation system design. In addition, he performs fundamental research in cycle ambiguity resolution with constrained integrity and fault detection and mitigation. Dr. Khanafseh received his PhD degree in mechanical and aerospace engineering from the Illinois Institute of Technology.

Boris Pervan is a professor of aerospace engineering at the Illinois Institute of Technology. His work pervades many fields of navigation research including: carrier phase DGPS, aircraft precision approach and landing, optimal and robust navigation system design, integrity monitoring and integration of inertial and laser sensors with GPS. Dr. Pervan received his PhD degree in aeronautics and astronautics from Stanford University.

ABSTRACT

This paper provides two algorithms to upper bound integrity risk in carrier phase differential GPS navigation systems that utilize cycle resolution. The measurement and process noise autocorrelation functions are known to lie between two specified functions but their precise mathematical nature is unknown. In previous work, an algorithm was developed to compute upper bounds on the integrity risk associated with a scalar linear combination of the estimate error vector given this bounded uncertainty structure. However, those algorithms are only applicable to floating carrier phase navigation systems. When cycle resolution is required, it becomes necessary to simultaneously consider the probability of correct ambiguity resolution. The performance of these two algorithms will be demonstrated for the benchmark application of autonomous shipboard landing.

INTRODUCTION

High accuracy aviation applications necessitate the use of carrier phase differential GPS with cycle resolution. When these applications are also life-critical, the navigation system must also simultaneously provide high levels of integrity. The integrity risk computation is based on the estimate error covariance matrix. When using a Kalman filter, the estimate error covariance matrix is only meaningful when the filter model exactly matches reality. Obtaining exact measurement and state dynamic models is exceedingly difficult, especially when the measurement and process noise time series are partially unknown.

Carrier phase multipath is one error source encountered in differential GPS navigation that is difficult to model. We know that this error source is time correlated, and can be reasonably modeled as a first order Gauss-Markov process. Until recently, it was commonly believed that using the largest permissible multipath time constant in the filter would produce an upper bound on the integrity risk. However, we showed in our prior work that this is not the case, and a more rigorous approach is required to upper bound integrity risk [1].

In reality we most likely don't know the precise mathematical structure of the measurement and process noise autocorrelation functions. A more realistic uncertainty structure is one where the input noise autocorrelation functions are contained between two prescribed functions. We considered this bounded uncertainty structure in [2] and showed how to upper bound the integrity risk of a scalar, linear combination of the state estimate error vector. The algorithm provided in [2] is applicable to floating differential carrier phase navigation systems, where integrity risk only depends on

the estimate error variance of the state of interest. Once cycle resolution is included in the algorithm, the integrity risk equation becomes significantly more complicated.

In the first part of this paper, we will show that integrity risk through cycle resolution depends on a vector of conditional variances. Each of these variances will be unknown due to the time series modeling uncertainty. We'll show that for the integer bootstrapped estimator, they can be written as an affine function of the unknown autocorrelation function values from which we can easily extract an upper and lower bound. A direct approach to upper bound the integrity risk is to set each of the conditional variances equal to their largest possible value. However, this approach does not account for the fact that the variances are all derived from the same input noise sequences. That is, they cannot be chosen independently.

The second part of this paper formulates the integrity risk bounding problem as a formal optimization problem. Unfortunately, it is non-convex and we cannot extract an efficient algorithm to find the global minimum. However, we will see that the cost function is a Schur-concave function. This special property allows us to use majorization inequalities to find the global minimum. The resulting algorithm is a two stage algorithm that requires the solution to a convex optimization problem prior to the majorization step. Although computationally more demanding, the resulting upper bound is shown to be less conservative than the direct bounding approach.

The algorithms developed in this work are applied to the benchmark application of autonomous shipboard landing. For a single approach, it will be shown that the integrity risk bound exceeds the requirement, in which case the approach is deemed unavailable. Furthermore, if the time series modeling uncertainty is accounted for using heuristic arguments, we would conclude that the approach has sufficient integrity to be initiated. This dangerous situation clearly demonstrates the need for the methods developed in this work to upper bound integrity risk through cycle resolution.

FUNDAMENTALS

We consider linear measurement and state dynamic models of the form

$$\boldsymbol{z}_k = \mathbf{H}_{\theta,k}\,\boldsymbol{\theta}_k + \mathbf{J}_{v,k}\,\boldsymbol{v}_k \tag{1}$$

$$\boldsymbol{\theta}_{k+1} = \mathbf{F}_{\theta,k}\,\boldsymbol{\theta}_k + \mathbf{G}_{\theta,k}\,\boldsymbol{w}_k \tag{2}$$

where $\boldsymbol{z}_k$ is an $n_z \times 1$ measurement vector, $\mathbf{H}_{\theta,k}$ is an $n_z \times n_\theta$ observation matrix, $\boldsymbol{\theta}_k$ is an $n_\theta \times 1$ state vector, $\mathbf{J}_{v,k}$ is an $n_z \times m$ measurement noise mapping matrix, $\boldsymbol{v}_k$ is an $m \times 1$ measurement noise vector, $\mathbf{F}_{\theta,k}$ is an $n_\theta \times n_\theta$ state transition matrix, $\mathbf{G}_{\theta,k}$ is an $n_\theta \times p$ process noise mapping matrix and $\boldsymbol{w}_k$ is a $p \times 1$ process noise vector. We assume that $\mathbf{H}_{\theta,k}$, $\mathbf{J}_{v,k}$, $\mathbf{F}_{\theta,k}$ and $\mathbf{G}_{\theta,k}$ are known matrices and that $\boldsymbol{v}_k$ and $\boldsymbol{w}_k$ are zero-mean Gaussian random noise vectors with the following properties

$$E[\boldsymbol{v}_k \boldsymbol{v}_l^T]_{ij} = \overset{v}{r}_{i,k-l}\,\delta_{ij} \tag{3}$$

$$E[\boldsymbol{w}_k \boldsymbol{w}_l^T]_{ij} = \overset{w}{r}_{i,k-l}\,\delta_{ij} \tag{4}$$

$$E[\boldsymbol{v}_k \boldsymbol{w}_l^T] = \mathbf{0} \quad , \quad \forall \;\; k \text{ and } l \tag{5}$$

where $\overset{v}{r}_{i,k-l}$ is the autocorrelation function of the measurement noise from sensor i evaluated at a time shift of $k-l$, $\overset{w}{r}_{i,k-l}$ is the autocorrelation function of disturbance input i evaluated at a time shift of $k-l$ and δ_{ij} is the Kronecker delta. The conditions in (3), (4) and (5) indicate that each measurement and process noise time series is auto-correlated, but is not cross-correlated with any other time series.

Together, (1) through (5) constitute the fundamental model that arises from our physical understanding of the sensors and system under consideration.

Before we can apply a Kalman filter to estimate $\boldsymbol{\theta}_k$, the colored nature of $\boldsymbol{v}_k$ and $\boldsymbol{w}_k$ must be accounted for. State augmentation is the most commonly used method for dealing with colored noise processes [3]. In this approach, $\boldsymbol{v}_k$ and $\boldsymbol{w}_k$ are modeled as the output of a linear system driven by white noise, which transforms the fundamental model to the following filter model

$$\boldsymbol{z}_k = \mathbf{H}_k\,\boldsymbol{x}_k + \mathbf{J}_k\,\boldsymbol{r}_k \tag{6}$$

$$\boldsymbol{x}_{k+1} = \mathbf{F}_k\,\boldsymbol{x}_k + \mathbf{G}_k\,\boldsymbol{q}_k \tag{7}$$

$$E[\boldsymbol{r}_k \boldsymbol{r}_l^T] = \mathbf{R}_k\,\delta_{kl} \tag{8}$$

$$E[\boldsymbol{q}_k \boldsymbol{q}_l^T] = \mathbf{Q}_k\,\delta_{kl} \tag{9}$$

$$E[\boldsymbol{r}_k \boldsymbol{q}_l^T] = \mathbf{0} \quad , \quad \forall \;\; k \text{ and } l \tag{10}$$

where $\mathbf{H}_k$ is an $n_z \times n_x$ matrix, $\boldsymbol{x}_k$ is an $n_x \times 1$ state vector, $\mathbf{J}_k$ is an $n_z \times n_r$ matrix, $\boldsymbol{r}_k$ is an $n_r \times 1$ white noise vector, $\mathbf{F}_k$ is an $n_x \times n_x$ matrix, $\mathbf{G}_k$ is an $n_x \times n_q$ matrix, $\boldsymbol{q}_k$ is an $n_q \times 1$ white noise vector and $\mathbf{R}_k$ and $\mathbf{Q}_k$ are the covariance matrices of $\boldsymbol{r}_k$ and $\boldsymbol{q}_k$, respectively.

Given that $\boldsymbol{v}_k$ and $\boldsymbol{w}_k$ are Gaussian random noise processes, the state estimate error vector $\boldsymbol{\varepsilon}_k$ is also a Gaussian random process

$$\boldsymbol{\varepsilon}_k \sim N(\mathbf{0}, \hat{\mathbf{P}}_x) \tag{11}$$

where $\hat{\mathbf{P}}_x$ is the estimate error covariance matrix output from the Kalman filter. That $\boldsymbol{\varepsilon}_k$ is zero-mean arises from the fact that the Kalman filter is an unbiased estimator.

A critical quantity that appears frequently in safety-of-life applications is integrity risk, defined as the probability of the estimate error residing outside a specified interval. Mathematically, integrity risk can be expressed as

$$I_y = P\left(|\varepsilon_y| \geq \ell_y \right) \tag{12}$$

where $y = \boldsymbol{\alpha}^T \mathbf{x}_k$ ($\boldsymbol{\alpha}$ known), ε_y is the estimate error of y distributed as $N(0\ ,\ \hat{\sigma}_y^2)$ and λ_y is a specified alert limit.

As long as $\hat{\sigma}_y^2$ is precisely known, it is straightforward to compute I_y. When the filter model is uncertain due to uncertainty in the statistical models of the measurement and process noise time series, $\hat{\sigma}_y^2$ is not an accurate descriptor of the probability distribution of ε_y. In this case, an upper bound on the *true* estimate error variance of y (denoted σ_y^2) is required to guarantee that I_y is bounded in the presence of uncertainty.

INTEGRITY RISK WITH UNCERTAINTY

In this work, we assume that the measurement noise and disturbance input autocorrelation functions are contained within a specified region. That is,

$$\overset{w}{a}_{i,k} \leq \overset{w}{r}_{i,k} \leq \overset{w}{b}_{i,k} \ , \ i = 1, \ldots, p \tag{13}$$

$$\overset{v}{a}_{j,k} \leq \overset{v}{r}_{j,k} \leq \overset{v}{b}_{j,k} \ , \ j = 1, \ldots, m \tag{14}$$

where the $\boldsymbol{a}$'s and $\boldsymbol{b}$'s are known. To assess the impact of the uncertainty structure in (13) and (14) on the estimate error, we derived the following expression in [2]

$$\boldsymbol{\varepsilon}_k = \boldsymbol{\Phi}_k \boldsymbol{\varepsilon}_0^- + \sum_{\substack{i=1 \\ k \neq 0}}^{p} \boldsymbol{\Gamma}_{i,k}^- \overline{\boldsymbol{w}}_i + \sum_{j=1}^{m} \boldsymbol{\Lambda}_{j,k}^- \overline{\boldsymbol{v}}_j \tag{15}$$

where $\boldsymbol{\varepsilon}_k$ is the estimate error vector using measurements up to and including time k, $\boldsymbol{\Phi}_k$ is an $n_x \times n_x$ matrix that maps the initial state estimate error vector to the current-time state estimate error vector, $\overline{\boldsymbol{w}}_i$ is an $n_{w,i} \times 1$ time series vector of disturbance input i from time $t = 0$ to $t = k$ and $\boldsymbol{\Gamma}_{i,k}^-$ is an $n_x \times n_{w,i}$ matrix that maps $\overline{\boldsymbol{w}}_i$ into $\boldsymbol{\varepsilon}_k$. Similarly, $\overline{\boldsymbol{v}}_j$ is an $n_{v,j} \times 1$ time series vector of the measurement error from sensor j and $\boldsymbol{\Lambda}_{j,k}^-$ is an $n_x \times n_{v,j}$ matrix that maps $\overline{\boldsymbol{v}}_j$ into $\boldsymbol{\varepsilon}_k$.

Details regarding how $\boldsymbol{\Phi}_k$, $\boldsymbol{\Gamma}_{i,k}^-$ and $\boldsymbol{\Lambda}_{j,k}^-$ are computed can be found in [2] and will not be repeated here. What is important is that these matrices are continually updated and modified after each step of the Kalman filter.

Time Update	Measurement Update
$\boldsymbol{\Phi}_{k+1}^- = \mathbf{A}_{k+1} \boldsymbol{\Phi}_k$	$\boldsymbol{\Phi}_{k+1} = \mathbf{C}_{k+1} \boldsymbol{\Phi}_{k+1}^-$
$\boldsymbol{\Gamma}_{i,k+1}^- = [\mathbf{A}_{k+1} \boldsymbol{\Gamma}_{i,k} \mid \boldsymbol{d}_{i,k}]$	$\boldsymbol{\Gamma}_{i,k+1} = \mathbf{C}_{k+1} \boldsymbol{\Gamma}_{i,k+1}^-$
$\boldsymbol{\Lambda}_{j,k+1}^- = \mathbf{A}_{k+1} \boldsymbol{\Lambda}_{j,k}$	$\boldsymbol{\Lambda}_{j,k+1} = [\mathbf{C}_{k+1} \boldsymbol{\Lambda}_{j,k+1}^- \mid \boldsymbol{b}_{j,k}]$

Table 1: Bounding algorithm update equations [2]

where $\mathbf{A}_{k+1}$, $\mathbf{C}_{k+1}$, $\boldsymbol{d}_{i,k}$ and $\boldsymbol{b}_{j,k}$ are derived from the filter model.

Notice that $\boldsymbol{\Phi}_k$, $\boldsymbol{\Gamma}_{i,k}$ and $\boldsymbol{\Lambda}_{j,k}$ are updated by $\mathbf{A}_{k+1}$ and a new column is appended to $\boldsymbol{\Gamma}_{i,k}$ after each time update. Similarly, $\boldsymbol{\Phi}_{k+1}^-$, $\boldsymbol{\Gamma}_{i,k+1}^-$ and $\boldsymbol{\Lambda}_{j,k+1}^-$ are updated by $\mathbf{C}_{k+1}$ and a new column is added to $\boldsymbol{\Lambda}_{j,k+1}^-$ after each measurement update.

The estimate error variance of y is obtained by evaluating $E[\boldsymbol{\varepsilon}_k \boldsymbol{\varepsilon}_k^T]$ and applying the covariance transformation law. When combining this step with equations (3), (4) and (5), it can be shown that [2]

$$\sigma_y^2 = \beta_y + \sum_{i=1}^{p} \sum_{s=0}^{n_{w,i}-1} \overset{w}{\gamma}_{i,s} \overset{w}{r}_{i,s} + \sum_{j=1}^{m} \sum_{u=0}^{n_{v,j}-1} \overset{v}{\gamma}_{j,u} \overset{v}{r}_{j,u} \tag{16}$$

where β_y, $\overset{w}{\gamma}_{i,s}$ and $\overset{v}{\gamma}_{j,u}$ are known coefficients.

Equation (16) will appear frequently throughout this paper, and hence is written more succinctly as

$$\sigma_y^2 = \beta_y + \boldsymbol{c}_y^T \boldsymbol{r} \tag{17}$$

where $\boldsymbol{r}$ is a column vector composed of all the $\overset{w}{r}_{i,s}$'s and $\overset{v}{r}_{j,u}$'s. Equation (17) allows us to incorporate the uncertainty structure from (13) and (14) in formulating an upper bound on σ_y^2. Specifically, if a given component of $\boldsymbol{c}_y$ is positive, then the corresponding component of $\boldsymbol{r}$ is set equal to its largest value. If the component of $\boldsymbol{c}_y$ is negative, the corresponding component of $\boldsymbol{r}$ is set equal to its smallest value. This procedure will produce the greatest upper bound on σ_y^2.

For the case where the probability distribution of ε_y is zero-mean Gaussian, we have seen that integrity risk depends on the single parameter, σ_y^2. However, there are instances where the distribution is not Gaussian, in which case integrity risk will depend on a vector of parameters. This occurs, for example, when there are integer constraints on certain elements of the state vector; a situation encountered in carrier phase differential GPS navigation. In the next section, an expression for integrity risk in mixed real / integer estimation is derived. As we'll see, the ability to write the estimate error variance in the form of (17) will play a critical role in establishing an upper bound on integrity risk for integer-constrained estimation problems.

MIXED REAL / INTEGER ESTIMATION

Suppose that the state vector can be written as

$$\boldsymbol{x}_k = [\, \boldsymbol{\xi}_{1,k}^T \;\; \boldsymbol{a}^T \,]^T \tag{18}$$

where $\boldsymbol{\xi}_{1,k}$ is a subset of the state vector whose components can take on any real number and $\boldsymbol{a}$ is a subset of the state vector that is constrained to be an integer vector. The Kalman filter provides us with a real-valued estimate of $\boldsymbol{a}$, denoted by $\hat{\boldsymbol{a}}$, that is distributed as

$$\hat{\boldsymbol{a}} \sim N(\boldsymbol{a}\,,\, \hat{\mathbf{P}}_a) \tag{19}$$

where $\hat{\mathbf{P}}_a$ is the estimate error covariance matrix of $\hat{\boldsymbol{a}}$.

The next step is to perform an integer resolution process that transforms $\hat{\boldsymbol{a}}$ to an integer estimate, $\breve{\boldsymbol{a}}$. Because $\hat{\boldsymbol{a}}$ is a random vector, there is a certain probability that $\breve{\boldsymbol{a}}$ will be resolved to the integer vector $\boldsymbol{d}$. Of course, this probability is dependent on how $\breve{\boldsymbol{a}}$ is formed. The effect of integer resolution on integrity risk is accounted for by using the fact that the set of all possible $\boldsymbol{d}$'s constitute a countably infinite set. In this case, the law of total probability can be used to write (12) in the form

$$I_y = \sum_{i=1}^{\infty} P\left(\,|\,\varepsilon_y\,| > \ell_y \,|\, \breve{\boldsymbol{a}} = \boldsymbol{d}_i\right) P\left(\breve{\boldsymbol{a}} = \boldsymbol{d}_i\right) \tag{20}$$

In this work, we make the conservative assumption that an incorrect resolution causes $|\,\varepsilon_y\,| > \ell_y$ with a probability of one. In mathematical terms

$$P\left(\,|\,\varepsilon_y\,| > \ell_y \,|\, \breve{\boldsymbol{a}} = \boldsymbol{d}_i\right) = 1 \;,\; \boldsymbol{d}_i \neq \boldsymbol{a} \tag{21}$$

Applying (21) to (20) and using the fact that

$$\sum_{i=2}^{\infty} P\left(\breve{\boldsymbol{a}} = \boldsymbol{d}_i\right) = 1 - P\left(\breve{\boldsymbol{a}} = \boldsymbol{a}\right) \tag{22}$$

allows I_y to be written in the form

$$I_y = 1 - \left[\, 1 - P\left(\,|\,\varepsilon_y\,| > \ell_y \,|\, \breve{\boldsymbol{a}} = \boldsymbol{a}\right)\right] P\left(\breve{\boldsymbol{a}} = \boldsymbol{a}\right) \tag{23}$$

which can finally be expressed as

$$I_y = 1 - P\left(\,|\,\varepsilon_y\,| \leq \ell_y \,|\, \breve{\boldsymbol{a}} = \boldsymbol{a}\right) P\left(\breve{\boldsymbol{a}} = \boldsymbol{a}\right) \tag{24}$$

In general, integer estimators fall into one of the following classes: integer rounding, integer bootstrapping and integer least squares, all of which are discussed thoroughly in [4]. The bootstrapped estimator is considered here due to its practical advantages. It is a sequential estimator and therefore allows us to control how many components of $\hat{\boldsymbol{a}}$ are resolved to an integer value; an appealing feature given that it may not be possible to resolve $\hat{\boldsymbol{a}}$ entirely to an integer vector without violating the integrity risk requirement.

INTEGER BOOTSTRAPPED ESTIMATOR

The fundamental premise behind integer bootstrapping is conditional least squares estimation [5]. The process begins by simply rounding the first component of $\hat{\boldsymbol{a}}$ to its nearest integer, $\breve{a}_1$. Because all of the components of $\hat{\boldsymbol{a}}$ are correlated, the information conveyed by the first integer resolution directly impacts the remaining components of $\hat{\boldsymbol{a}}$. This effect is captured by updating $\hat{\boldsymbol{a}}$ and $\hat{\mathbf{P}}_a$ to the conditional quantities $\hat{\boldsymbol{a}}_{|1}$ and $\hat{\mathbf{P}}_{a|1}$, respectively, where the notation " | 1" indicates that the first component of $\hat{\boldsymbol{a}}$ has been resolved to an integer. Next, the second component of $\hat{\boldsymbol{a}}_{|1}$ is rounded to its nearest integer, $\breve{a}_{2|1}$ followed by an update of $\hat{\boldsymbol{a}}_{|1}$ and $\hat{\mathbf{P}}_{a|1}$ to $\hat{\boldsymbol{a}}_{|2,1}$ and $\hat{\mathbf{P}}_{a|2,1}$, respectively. This process is continued until the desired number of components have been resolved to integer values.

It is not necessary to constrain the integer resolution process exclusively to the original components of $\hat{\boldsymbol{a}}$. In general, we can resolve the components of any linear transformation of $\hat{\boldsymbol{a}}$, as long as that transformation preserves the integer nature of $\boldsymbol{a}$. Teunissen has shown that if we choose a linear transformation (denoted by $\mathbf{Z}$) that decorrelates $\hat{\mathbf{P}}_a$, the probability of resolving the integers correctly is improved significantly [6]. Therefore, $\hat{\boldsymbol{a}}$ and $\hat{\mathbf{P}}_a$ are transformed to the new quantities $\hat{\boldsymbol{b}} = \mathbf{Z}\hat{\boldsymbol{a}}$ and $\hat{\mathbf{P}}_b = \mathbf{Z}\hat{\mathbf{P}}_a\,\mathbf{Z}^T$ prior to bootstrapping.

In what follows we will continue to denote the integer component of the state vector by $\boldsymbol{a}$ with the understanding that the decorrelation procedure described above has already been performed. For the bootstrapped estimator, the probability of resolving $\hat{\boldsymbol{a}}$ to the correct integer vector $\boldsymbol{a}$ is given by [5]

$$P\left(\breve{\boldsymbol{a}}=\boldsymbol{a}\right)=\prod_{q=1}^{n}\left[2\boldsymbol{\Phi}\left(\frac{1}{2\sigma_{q|q-1}}\right)-1\right] \qquad (25)$$

where $\sigma^2_{q|q-1}$ is the conditional variance of the q^{th} component of $\hat{\boldsymbol{a}}$ given that the $q-1$ previous components have been resolved to integers and n is the total number of components of $\hat{\boldsymbol{a}}$ resolved to an integer value. $\boldsymbol{\Phi}(x)$ is the standard normal cumulative distribution function

$$\boldsymbol{\Phi}(x)=\int_{-\infty}^{x}\frac{1}{\sqrt{2\pi}}\exp\left(-\frac{1}{2}v^2\right)dv \qquad (26)$$

The conditional distribution of ε_y after integer resolution is zero-mean Gaussian with conditional variance $\sigma^2_{y|n}$, and therefore we can write

$$P\left(|\,\varepsilon_y\,|\le\ell_y\,|\,\breve{\boldsymbol{a}}=\boldsymbol{a}\right)=\left[2\boldsymbol{\Phi}\left(\frac{\ell_y}{\sigma_{y|n}}\right)-1\right] \qquad (27)$$

Inserting (25) and (27) into (24) and expressing $\boldsymbol{\Phi}(x)$ in terms of the error function results in

$$I_y=1-\text{erf}\left(\frac{\ell_y}{\sqrt{2\sigma^2_{y|n}}}\right)\prod_{q=1}^{n}\text{erf}\left(\frac{1/2}{\sqrt{2\sigma^2_{q|q-1}}}\right) \qquad (28)$$

From (28), it is clear that I_y is a function of a vector of conditional variances, each of which is unknown in the presence of time series modeling uncertainty. In the next section we will show that integer bootstrapping can be formulated as a pseudo-measurement update. This will allow us to express each of the conditional variances in the linear form of (17).

UPDATE FORM OF INTEGER BOOTSTRAPPING

It is shown in [5] that $\sigma^2_{q|q-1}$ can be obtained directly from an $\mathbf{LDL}^T$ decomposition of $\hat{\mathbf{P}}_a$. An alternative approach to computing $\sigma^2_{q|q-1}$ that meshes well with our previous work is to view each step of the bootstrapping process as a pseudo-measurement update. To see this, consider the first step of bootstrapping, where $\hat{a}_1$ is resolved to the value $\breve{a}_1$. We can view $\breve{a}_1$ as a noise-free measurement of a_1, with measurement model

$$\breve{a}_1=[\,\mathbf{0}\quad\mathbf{Z}_1\quad\mathbf{0}\,]\boldsymbol{x}_k \qquad (29)$$

where $\mathbf{Z}_1$ is the first row of the transformation matrix, $\mathbf{Z}$.

Performing a measurement update with (29) yields the conditional quantities $\hat{\boldsymbol{x}}_{k|1}$ and $\hat{\mathbf{P}}_{x|1}$, from which we can easily extract $\hat{\boldsymbol{a}}_{|1}$ and $\hat{\mathbf{P}}_{a|1}$. The fact that $\hat{\boldsymbol{a}}_{|1}$ and $\hat{\mathbf{P}}_{a|1}$ can be obtained through a measurement update implies that $\boldsymbol{\Phi}_k$, $\boldsymbol{\Gamma}_{i,k}$ and $\boldsymbol{\Lambda}_{j,k}$ can be updated as described in table I to reflect integer resolution. However, because (29) is a noise-free measurement, we do not append a new column to $\boldsymbol{\Lambda}_{j,k}$. In general, we have the following results

$$\boldsymbol{\Phi}_{k|q}=\mathbf{C}_{k|q}\boldsymbol{\Phi}_{k|q-1} \qquad (30a)$$

$$\boldsymbol{\Gamma}_{i,k|q}=\mathbf{C}_{k|q}\boldsymbol{\Gamma}_{i,k|q-1} \qquad (30b)$$

$$\boldsymbol{\Lambda}_{j,k|q}=\mathbf{C}_{k|q}\boldsymbol{\Lambda}_{j,k|q-1} \qquad (30c)$$

Once we've obtained $\boldsymbol{\Phi}_{k|q}$, $\boldsymbol{\Gamma}_{i,k|q}$ and $\boldsymbol{\Lambda}_{j,k|q}$, the algorithm from [1] is applied to express the conditional variances in terms of the unknown vector, $\boldsymbol{r}$.

UPPER BOUNDING INTEGRITY RISK THROUGH INTEGER RESOLUTION

The integrity risk equation provided in (28) can be written in the generic form

$$I_y=1-\text{erf}\left(\frac{1}{\sqrt{2\varphi_0}}\right)\ldots\text{erf}\left(\frac{1}{\sqrt{2\varphi_n}}\right) \qquad (31)$$

where $\varphi_0,\ldots,\varphi_n$ are uncertain parameters. From the discussion following (17), we know that we can upper and lower bound each of the φ_i's given the uncertainty structure in (13) and (14). If we set the φ_i's equal to their largest permissible value, we will certainly minimize the product of error functions which in turn will result in an upper bound on I_y. However, this *direct bounding approach* does not account for the fact that the φ_i's are all derived from the same $\boldsymbol{r}$ vector. That is, $\varphi_0,\ldots,\varphi_n$ cannot be chosen independently and instead must comply with a certain set of constraints. In order to illustrate the nature of the constraints, consider the following example.

$$\begin{bmatrix}\varphi_0\\ \varphi_1\end{bmatrix}=\begin{bmatrix}1\\ 1\end{bmatrix}+\begin{bmatrix}2 & 1 & -1\\ 1 & -1 & 2\end{bmatrix}\begin{bmatrix}r_0\\ r_1\\ r_2\end{bmatrix},\ \begin{cases}1\le r_0\le 2\\ 0.75\le r_1\le 1.75\\ 0.5\le r_2\le 1.5\end{cases} \qquad (32)$$

First, notice that φ_0 and φ_1 are in the form of (17) and that the components of $\boldsymbol{r}$ have the bounded uncertainty structure of (13) and (14). Mapping the three-dimensional

box from the $\boldsymbol{r}$ domain to the (φ_0, φ_1) domain results in the blue feasible region shown in figure 1.

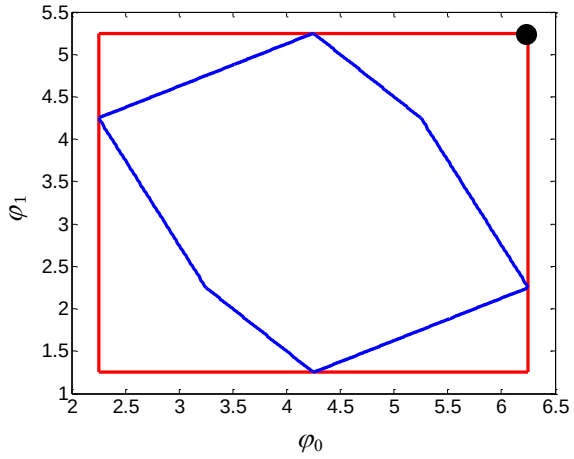

Figure 1: Feasible regions, where the red box is a conservative approximation of the true region in blue.

The black dot is the point we select to upper bound I_y in the direct bounding approach. However, this point may be far removed from the actual feasible region, resulting in an overly conservative integrity risk bound.

If we wish to work with the true feasible region, there are two difficulties that need to be addressed. First, the number of operations required to perform the mapping from the $\boldsymbol{r}$ domain to the $\boldsymbol{\varphi}$ domain increases substantially as the size of $\boldsymbol{r}$ increases. Second, in order to compute the integrity risk bound, we must solve the optimization problem

$$\phi_y^* = \min_{\boldsymbol{\varphi}} \ \operatorname{erf}\left(\frac{1}{\sqrt{2\varphi_0}}\right) \ldots \operatorname{erf}\left(\frac{1}{\sqrt{2\varphi_n}}\right) \qquad (33)$$

$$\text{s.t} \quad \mathbf{A}_i \boldsymbol{\varphi} \le \boldsymbol{b}_i \quad , \quad i = 1, \ldots, N$$

where $\mathbf{A}_i$ and $\boldsymbol{b}_i$ are determined from the mapping process and N is the total number of linear constraints. Unfortunately, the cost function in (33) is not a convex function. This is most easily seen by noting that a composition of convex functions is itself a convex function [7].

Suppose that we have two φ variables and that we can express φ_0 in terms of φ_1.

$$\begin{bmatrix} \varphi_0 \\ \varphi_1 \end{bmatrix} = \begin{bmatrix} u_0 \\ 0 \end{bmatrix} + \begin{bmatrix} v_0 \\ 1 \end{bmatrix} \varphi_1 \qquad (34)$$

Then the cost function can be written in the form

$$\phi_y = \operatorname{erf}\left(\frac{1}{\sqrt{2(u_0 + v_0 \varphi_1)}}\right) \operatorname{erf}\left(\frac{1}{\sqrt{2\varphi_1}}\right) \qquad (35)$$

Figure two shows a typical realization of ϕ_y for given values of u_0 and v_0.

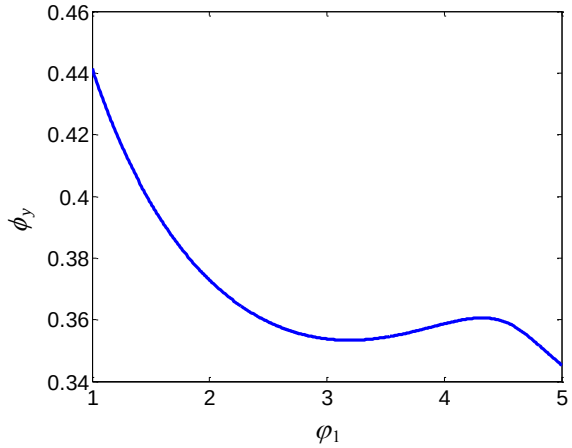

Figure 2: Realization of ϕ_y with $u_0 = 1.45$ and $v_0 = -0.29$.

Clearly, ϕ_y is not a convex function of φ_1. Because the composition is not a convex function, ϕ_y is not convex in $\boldsymbol{\varphi}$. Therefore, at best we will only be able to obtain a local minimum. For integrity risk bounding, local minima are not sufficient. If we were to converge on the local minimum at $\varphi_1 \approx 3.2$, we would not be upper bounding the integrity risk, which will occur when $\varphi_1 = 5$.

Given the difficulties described above, it is not possible to extract an efficient algorithm to upper bound integrity risk over the blue feasible region in figure 1. However, the cost function in (33) does possess a certain type of convexity. In the next section, we will exploit this structure to obtain a tight upper bound on integrity risk.

SCHUR CONCAVITY AND MAJORIZATION

It can be shown that the cost function in (33) is a Schur concave function in the following vector [8]

$$\boldsymbol{\rho} = \left[\frac{1}{\sqrt{\varphi_0}} \quad \frac{1}{\sqrt{\varphi_1}} \quad \cdots \quad \frac{1}{\sqrt{\varphi_n}}\right]^T \qquad (36)$$

A Schur concave function has the special property that

$$\boldsymbol{\rho}_1 \prec \boldsymbol{\rho}_2 \ \Rightarrow \ \phi(\boldsymbol{\rho}_1) \ge \phi(\boldsymbol{\rho}_2) \qquad (37)$$

where the symbol $\prec$ indicates majorization. That is, if $\boldsymbol{\rho}_2$ majorizes $\boldsymbol{\rho}_1$, then $\phi(\boldsymbol{\rho}_2)$ is smaller than $\phi(\boldsymbol{\rho}_1)$.

Mathematically, we say that $\boldsymbol{x}$ is majorized by $\boldsymbol{y}$ if [9]

$$\sum_{i=1}^{k} x_{[i]} \le \sum_{i=1}^{k} y_{[i]} \;,\; k = 1, \ldots, n-1$$
$$\sum_{i=1}^{n} x_{[i]} = \sum_{i=1}^{n} y_{[i]} \qquad (38)$$

The vector $[x_{[1]}, \ldots, x_{[n]}]^T$ is the decreasing rearrangement of $\boldsymbol{x}$. That is, $x_{[1]} \ge \ldots \ge x_{[n]}$.

What (37) really implies is that if we can find a vector $\boldsymbol{\rho}^*$ that majorizes every other vector, then we will obtain the global minimum solution to (33). However, there are a number of difficulties that must be addressed. First, we are working with a new variable $\boldsymbol{\rho}$ that is a nonlinear transformation of the original variable, $\boldsymbol{\varphi}$. This means that each of the linear constraints defining the feasible region in figure 1 will be transformed to nonlinear constraints. The second difficulty is that the majorization definition given in (38) implies that the sum of the components of $\boldsymbol{\rho}$ must be constant. The third issue is that in general there is not a single vector that will majorize every other vector in a given set. Only in certain specialized cases is this true.

Given upper and lower bounds on φ_i, we can easily create an upper and lower bound on ρ_i. We can also find a lower bound on the sum of the components of $\boldsymbol{\rho}$ by solving the following optimization problem

$$s^* = \min_{\boldsymbol{r}} \; \frac{1}{\sqrt{2(\beta_0 + \boldsymbol{c}_0^T \boldsymbol{r})}} + \ldots + \frac{1}{\sqrt{2(\beta_n + \boldsymbol{c}_n^T \boldsymbol{r})}} \qquad (39)$$
$$\text{s.t} \quad a_i \le r_i \le b_i \quad , \quad i = 1, \ldots, N$$

Equation (39) is a convex optimization problem that can be solved using any of the methods described in [7] and [10]. We only need a lower bound on the sum of the components of $\boldsymbol{\rho}$ because that will yield the smallest value of ϕ_y. Therefore, we must now solve the following problem

$$\phi_y^* = \min_{\boldsymbol{\rho}} \; \operatorname{erf}\left(\frac{\rho_0}{\sqrt{2}}\right) \ldots \operatorname{erf}\left(\frac{\rho_n}{\sqrt{2}}\right)$$
$$\text{s.t} \quad \ell_i \le \rho_i \le u_i \quad , \quad i = 0, \ldots, n \qquad (40)$$
$$\rho_0 + \ldots + \rho_n = s^*$$

The reader should be aware that the constraints in (40) are a conservative representation of the true feasible region. Using the result from [11], the optimal solution to (40) is given by

$$\boldsymbol{\rho}^* = \boldsymbol{u} \circ \boldsymbol{s}^k + \theta \boldsymbol{e}^{k+1} + \boldsymbol{\lambda} \circ \boldsymbol{v}^{k+1} \qquad (41)$$

where $\boldsymbol{u}$ is the vector of upper bounds arranged in nonincreasing order, $\boldsymbol{\lambda}$ is the vector of lower bounds arranged in nonincreasing order, $\boldsymbol{e}^j$, j = 1, . . . , n are the fundamental vectors of P^n and $\boldsymbol{s}^k$ and $\boldsymbol{v}^k$ are defined as

$$\boldsymbol{s}^0 = \boldsymbol{0} \;,\; \boldsymbol{s}^j = \sum_{i=1}^{j} \boldsymbol{e}^i \;,\; j = 1, \ldots, n \qquad (42)$$

$$\boldsymbol{v}^n = \boldsymbol{0} \;,\; \boldsymbol{v}^j = \sum_{i=j+1}^{n} \boldsymbol{e}^i \;,\; j = 0, \ldots, (n-1) \qquad (43)$$

The symbol $\circ$ indicates the Hadamard product of two vectors and k is the smallest integer such that

$$\left\langle \boldsymbol{u} \;,\; \boldsymbol{s}^k \right\rangle + \left\langle \boldsymbol{\lambda} \;,\; \boldsymbol{v}^k \right\rangle \le s^* \le \left\langle \boldsymbol{u} \;,\; \boldsymbol{s}^{k+1} \right\rangle + \left\langle \boldsymbol{\lambda} \;,\; \boldsymbol{v}^{k+1} \right\rangle \qquad (44)$$

where the angle brackets denote the Euclidean inner product. Finally, the scalar θ in (41) is given by

$$\theta = s^* - \left\langle \boldsymbol{u} \;,\; \boldsymbol{s}^k \right\rangle - \left\langle \boldsymbol{\lambda} \;,\; \boldsymbol{v}^{k+1} \right\rangle \qquad (45)$$

We now have two algorithms to compute an upper bound on integrity risk through cycle resolution: the direct bounding approach and the majorization bounding approach. With majorization inequalities, we must solve a convex optimization problem prior to computing $\boldsymbol{\rho}^*$ from (41). However, the increased computational burden will result in a tighter integrity risk bound, ultimately leading to high system availability. In the next section, we will demonstrate performance of these two approaches for the benchmark application of shipboard landing.

SHIPBOARD LANDING APPLICATION

Consider the scenario shown in figure 3.

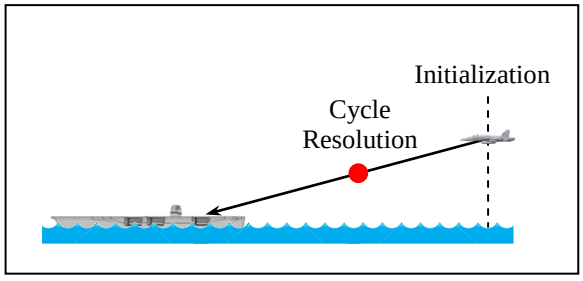

Figure 3: Shipboard landing problem setup

Assume that the aircraft and ship are equipped with dual frequency receivers. Then the relative position vector between the two vehicles can be estimated using double difference widelane carrier phase measurements. Ambiguity resolution is performed after ten measurement epochs, which are each separated by thirty seconds to capture the effect of satellite motion. In what follows, a

single satellite geometry will be simulated from the do229a 24–SV almanac.

With m satellites visible to both the aircraft and ship, the double difference widelane carrier phase measurement model is given by

$$\Delta^2\boldsymbol{\phi}_{\mathrm{WL},k} = [\,\mathbf{G}_k \quad \lambda_{\mathrm{WL}}\mathbf{I} \quad \mathbf{D}\,]\boldsymbol{x}_k + \mathbf{D}\boldsymbol{r}_k \qquad (46)$$

where $\Delta^2\boldsymbol{\phi}_{\mathrm{WL},k}$ is an $(m-1)\times 1$ measurement vector, $\mathbf{G}_k$ is an $(m-1)\times 3$ double difference geometry matrix, λ_{WL} is the widelane carrier wavelength, $\mathbf{I}$ is the $(m-1)\times(m-1)$ identity matrix, $\mathbf{D}$ is the $(m-1)\times m$ double difference transformation matrix and $\boldsymbol{r}_k$ is an $m\times 1$ white measurement noise vector.

The state vector $\boldsymbol{x}_k$ has dimension $(3+2m-1)\times 1$ and is composed of the relative position vector, the double difference widelane cycle ambiguities and the single difference widelane carrier phase multipath error states.

$$\boldsymbol{x}_k = [\,\Delta\boldsymbol{x}_k^T \quad \Delta^2\boldsymbol{n}_{\mathrm{WL}}^T \quad \Delta\boldsymbol{m}_{\mathrm{WL},k}^T\,]^T \qquad (47)$$

The state vector evolves according to the linear model

$$\begin{bmatrix} \Delta\boldsymbol{x} \\ \Delta^2\boldsymbol{n}_{\mathrm{WL}} \\ \Delta\boldsymbol{m}_{\mathrm{WL}} \end{bmatrix}_{k+1} = \begin{bmatrix} \mathbf{I} & \mathbf{0} & \mathbf{0} \\ \mathbf{0} & \mathbf{I} & \mathbf{0} \\ \mathbf{0} & \mathbf{0} & e^{-T/\tau}\mathbf{I} \end{bmatrix} \begin{bmatrix} \Delta\boldsymbol{x} \\ \Delta^2\boldsymbol{n}_{\mathrm{WL}} \\ \Delta\boldsymbol{m}_{\mathrm{WL}} \end{bmatrix}_k + \begin{bmatrix} \boldsymbol{\infty} \\ \mathbf{0} \\ \boldsymbol{w}_m \end{bmatrix} \qquad (48)$$

Notice from (48) that there is infinite process noise on the position state. This is done to reflect the fact that we do not have an adequate dynamic model for the relative position vector. Also notice that the multipath error states are modeled as first order Gauss-Markov random processes with time constant, τ.

The initial estimate error covariance matrix is given by

$$\mathbf{P}_0 = \begin{bmatrix} (100\,\mathrm{m}^2)\mathbf{I} & \mathbf{0} & \mathbf{0} \\ \mathbf{0} & (0.14^2)\mathbf{I} & \mathbf{0} \\ \mathbf{0} & \mathbf{0} & \sigma_m^2\mathbf{I} \end{bmatrix} \qquad (49)$$

A tight initial ambiguity covariance of $(0.14\text{ cycles})^2$ is used in this work so that we can resolve the cycle ambiguities with sufficient integrity at the fixing point. One way to obtain such a covariance is through geometry-free prefiltering [1]. The geometry-free measurement eliminates ionospheric and tropospheric error sources which allow the aircraft and ship to estimate floating widelane cycle ambiguities with high integrity prior to filter initialization.

Relevant simulation parameters are provided in table 2.

Parameter	Value
Measurement sampling rate	T = 30 sec
Cycle resolution point	t_{fix} = 300 sec
SD multipath error (1σ)	7 cm
SD multipath time constant	1800 sec
Measurement noise (1σ)	0 m
Satellite constellation	do229a (24 SV)
Vertical alert limit (λ_y)	1 m
Integrity risk requirement	3×10^{-7}

Table 2: Filter parameters used in simulation

For the bounding algorithms, we require an upper and lower bound on the single difference widelane carrier phase measurement noise autocorrelation function. In this example, we will use two exponential bounding functions, each with the following form

$$\overset{v}{a}_{j,k} = \sigma_a^2 \exp\left(-\frac{|k|T}{\tau_a}\right) \qquad (50a)$$

$$\overset{v}{b}_{j,k} = \sigma_b^2 \exp\left(-\frac{|k|T}{\tau_b}\right) \qquad (50b)$$

where $\sigma_a = 5.7\,\mathrm{cm}$, $\tau_a = 900\,\mathrm{s}$, $\sigma_b = 7\,\mathrm{cm}$ and $\tau_b = 1800\,\mathrm{s}$.

Notice that the filter multipath model uses the parameters corresponding to the upper autocorrelation bounding function. This will allow us to compare current heuristics to the bounding algorithms developed in this work.

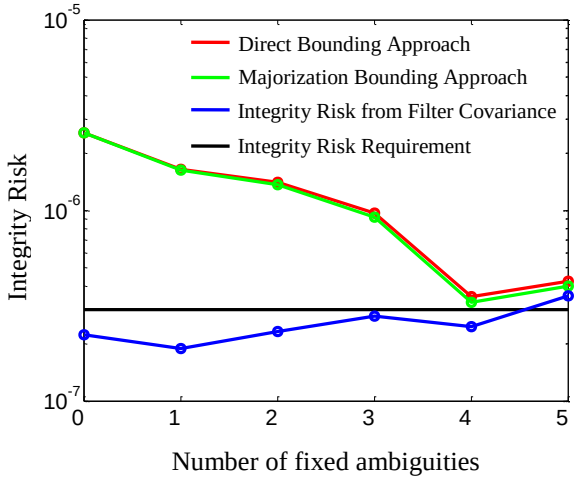

Figure 4: Simulation results for one aircraft approach

The most obvious conclusion from figure 4 is that the majorization bounding method does not provide much improvement over the direct bounding approach. Both

methods lead to the conclusion that this particular approach does not have sufficient integrity and therefore should not be initiated. What is most concerning about this example are the ramifications of failing to rigorously address time series modeling uncertainty. The blue curve is the integrity risk that would be computed using the covariance matrix output from the Kalman filter. Even though the filter uses the maximum variance and time constant to model multipath, we drastically under-represent the worst-case integrity risk. In fact, we would conclude that it is not even necessary to fix the cycle ambiguities. This example clearly illustrates the need for our algorithms to upper bound integrity risk through cycle resolution.

CONCLUSIONS

In this paper we provided two approaches to upper bound the integrity risk in carrier phase navigation systems that utilize cycle resolution. We showed that integer bootstrapping can be formulated as a pseudo-measurement update. This allowed us to express the conditional variances as an affine function of the unknown autocorrelation function values. A direct bounding approach that selects the maximum value of the conditional variances was initially proposed. However, this approach does not incorporate the linear inequality constraints that exist among the variances. In response, we developed a second algorithm based on majorization inequalities. This method does introduce a linear constraint, but we must solve a convex optimization problem prior to obtaining the integrity risk bound.

For the shipboard landing application, it was shown that the majorization approach does provide a slightly tighter bound over the direct approach. A very important assumption used in this research is that all incorrect fixes cause the estimate error to exceed the acceptable limit. This assumption is a conservative one, and more recent cycle resolution algorithms consider incorrect fix candidates together with the correct fix [12]. It is believed that the benefit of the majorizaton bounding approach will become apparent in these approaches. However, more analysis is required to test this hypothesis, and will be the focus of future efforts in this research.

ACKNOWLEDGMENTS

We would like to thank our research sponsors at Naval Air Systems Command (NAVAIR) for their continued support of this research effort.

REFERENCES

[1] S. Langel, S. Khanafseh and B. Pervan, "Bounding Integrity Risk in the Presence of Parametric Time Correlation Uncertainty," in *Proc. of the 2012 Int. Tech. Meeting of the Institute of Navigation*, CA, 2012, pp. 1666–1680.

[2] S. Langel, S. Khanafseh and B. Pervan, "Bounding Integrity Risk Subject to Structured Time Correlation Modeling Uncertainty," in *Proc. of the IEEE/ION Position, Location and Navigation Symposium*, SC, 2012, pp. 678 – 684.

[3] B.D.O Anderson and J.B Moore. *Optimal Filtering*, New York: Dover Publications, Inc., 1979.

[4] S. Verhagen. *The GNSS Integer Ambiguities: Estimation and Validation*, Delft, The Netherlands: Netherlands Geodetic Commission, 2005.

[5] P.J.G. Teunissen, "GNSS Ambiguity Bootstrapping: Theory and Application," in *Proc. of KIS*, Canada, 2001, pp. 246 – 254.

[6] P.J.G. Teunissen, "The Least-Squares Ambiguity Decorrelation Adjustment: A Method for Fast GPS Integer Ambiguity Estimation," *Journal of Geodesy*, vol. 70, no. 1–2, pp. 65 – 82, 1995.

[7] S. Boyd and L. Vandenberghe. *Convex Optimization*, New York: Cambridge University Press, 2004.

[8] Y.L. Tong, "Some Majorization Inequalities in Multivariate Statistical Analysis," *SIAM Review*, vol. 30, no. 4, pp. 602 – 622, 1988.

[9] A.W. Marshall and I. Olkin. *Inequalities: Theory of Majorization and Its Applications*, New York: Academic Press, Inc., 1979.

[10] D. G. Luenberger and Y. Ye. *Linear and Nonlinear* Programming, 3rd ed. New York: Springer, 2008.

[11] M. Bianchi et al, "Majorization Under Constraints and Bounds of the Second Zagreb Index," Contributi di Ricerca in Econometria e Matematica, 2011.

[12] S. Khanafseh and B. Pervan, "A New Approach for Calculating Position Domain Integrity Risk for Cycle Resolution in Carrier Phase Navigation Systems," *in Proc. of the IEEE Position, Location, and Navigation Symposium*, CA, 2008.